

## Magnetic inversion symmetry breaking and spin reorientation in $\text{Tb}_2\text{MnNiO}_6$ : A polar strong ferromagnet

Jose Luis García-Muñoz,<sup>1,\*</sup> Javier Blasco,<sup>2</sup> Xiaodong Zhang,<sup>1</sup> and Oscar Fabelo<sup>3</sup>

<sup>1</sup>*Institut de Ciència de Materials de Barcelona, ICMAB-CSIC, Campus Universitari de Bellaterra, E-08193 Bellaterra, Spain*

<sup>2</sup>*Instituto de Ciencia de Materiales de Aragón, Departamento de Física de la Materia Condensada, Consejo Superior de Investigaciones Científicas (CSIC)—Universidad de Zaragoza, E-50009 Zaragoza, Spain*

<sup>3</sup>*ILL-Institut Laue Langevin, 71, Avenue des Martyrs, 38042 Grenoble Cedex, France*



(Received 3 March 2019; revised manuscript received 5 May 2019; published 29 May 2019)

We report a description and comprehensive study on four successive magnetic transitions in ferromagnetic  $\text{Tb}_2\text{MnNiO}_6$  double perovskite. In the ground state ( $P2'_1$ ), the moments of magnetic  $A$  and  $B$  sites order according to different nonpolar magnetic modes, but the coupling between them generates an overall polar symmetry which makes this oxide potentially multiferroic due to magnetic trilinear coupling, and therefore ferromagnetic and ferroelectric in its ground state. Its macroscopic magnetization is large ( $5 \mu_B/\text{f.u.}$ ) and not related to a weak ferromagnetic component induced by Dzyaloshinskii-Moriya interaction. However, a sharp and severe spin reorientation of the ferromagnetic transition-metal moments has been observed which opens the door to the magnetic switching of the ferroelectric state in this perovskite, and conversely to the control of the magnetization direction by electrical fields applied parallel to  $b$ . We also anticipate that in this material the direction of the magnetization (towards  $c/a$ ) could be used as the key to switch the polar/nonpolar (ferroelectric/antiferroelectric) transformation.

DOI: [10.1103/PhysRevB.99.184444](https://doi.org/10.1103/PhysRevB.99.184444)

### I. INTRODUCTION

Unlike the proper ferroelectrics, in improper ferroelectrics the polarization ( $P$ ) does not arise from the condensation of a polar lattice distortion associated to a zone-center instability but it is a secondary effect induced by some other primary distortion  $D$  that introduces an odd coupling of the polar and nonpolar modes (free-energy term of the form  $F = \alpha PD^n$ ). If  $n$  is odd the polarization can switch by inverting the distortion mode  $D$ . Let us recall first that the appearance of ferroelectricity induced by antiferromagnetic transitions, which double the unit cell, has attracted attention for a long time [1]. Like other effects described by tensors which are invariants under time reversal, it was predicted to appear accompanying the reduction of symmetry associated with magnetic transitions. Therefore, it is known that in materials such as perovskites, the presence of magnetic atoms at special Wyckoff positions can favor a polar magnetic symmetry [2]. For example, in compounds with nonsymmorphic space groups, if the magnetic atoms sit at special Wyckoff positions (e.g., with point-group symmetry  $-1$ , as the monoclinic  $R_2\text{MnMO}_6$  [ $M$ : Ni, Co] series), some propagation vectors at the zone boundary of the paraelectric phase favor polar symmetries and the occurrence of type II multiferroicity. An example is the collinear  $E$  phase in monoclinic  $P2_1/n$  double perovskites (DPs) presenting up-up-down-down ( $\uparrow\uparrow\downarrow\downarrow$ ) spin chains along a particular crystallographic direction (e.g.,  $R_2\text{MnCoO}_6$ ,  $R = \text{Yb, Lu}$  [3]). The presence of a magnetic propagation vector  $\mathbf{k} = (0, 0, 1/2)$  implies that the glide plane is necessarily broken. The system can either keep the twofold screw rotation axis or the inversion

center, but not both. The propagation vector hosts the *anti-translation*  $\{1'|0\ 0\ 1\}$  in the parent setting [ $(1'|0,0,1/2)$  in the doubled magnetic cell], and the presence of opposite spins in contiguous parent unit cells is not compatible with the glide plane. The pristine point symmetry  $-1$  at the  $2c$  and  $2d$  sites ( $B, B'$ ) occupied by transition-metal atoms ( $M$ ) is lost as the  $E$ -type ordering requires both  $-11'$  and  $-1$  symmetry, depending on the considered spin.

However, this effective mechanism favoring the symmetry break into polar symmetries cannot be generalized to the cases in which the primary magnetic mode or cooperative atomic displacement  $R$  occurs at the point  $\mathbf{k} = 0$  (zone center) in the reciprocal space of the paraelectric phase, without an enlargement of the unit cell. In this case, the absence of changes in the translational symmetry precludes an antitranslation of the type  $\{1'|0\ 0\ n\}$  ( $n$ : integer, in the parent setting) able to break the point symmetry  $-1$ . In addition, it is worth remembering that conversely the cases with  $\mathbf{k} = 0$  can be more favorable to the presence of ferromagnetic (FM) configurations.

Secondly, the presence of magnetic atoms at the  $A$  site ( $R = \text{Tb}$  in the present case) and the coupling between the  $A$  and  $B$  spin subsystems in  $ABO_3$  like perovskites and their derived structures are cause for a variety of exciting effects [4]. In  $\text{RMO}_3$  compounds, the transition-metal spins order first because they interact stronger, although the spins of rare-earth ions can be much more anisotropic. The interactions between transition-metal and rare-earth spins are attracting interest due to their important effects in multiferroic and magnetoelectric materials [5]. In  $\text{DyFeO}_3$  a strong linear magnetoelectric response activates due to the interplay between the ordered spins of Fe and Dy ions [6]. In  $\text{GdFeO}_3$  orthoferrite the polar distortion producing spontaneous polarization results from the combination of the rotational  $Pbnm$  distortion and the

\*garcia.munoz@icmab.es

simultaneous G-AFM magnetic order of the independent Gd and Fe spin sublattices [4]. In the multiferroic  $\text{TbMnO}_3$  the coupling between the Mn spins produces a spin-density wave and later a spiral ferroelectric state. The ordering of Ising-like Tb spins below  $\sim 7$  K produces a mutual locking of the Mn and Tb spins and leads to a significant enhancement of the electric polarization induced by the spiral [7–9].

In this work, we report a description and comprehensive study on four successive magnetic transitions in the ferromagnetic  $\text{Tb}_2\text{MnNiO}_6$  DP driven by zone-center modes of the parent paramagnetic phase. In the ground state, the moments of magnetic  $A$  and  $B$  sites order according to different non-polar magnetic modes. However, the coupling between them generates an overall polar symmetry which makes this oxide potentially multiferroic due to magnetic trilinear coupling, and therefore a ferromagnetic ferroelectric in its ground state. A sharp spin reorientation of the ferromagnetic transition-metal moments has been observed which opens the door to the magnetic switching of the ferroelectric state in this perovskite.

## II. EXPERIMENTAL SECTION

The  $\text{Tb}_2\text{MnNiO}_6$  double perovskite was prepared by the conventional solid-state reaction method. Stoichiometric amounts of  $\text{Tb}_4\text{O}_7$ , NiO, and  $\text{Mn}_2\text{O}_3$  with nominal purities not less than 99.9% were mixed, ground, and heated for 15 h at  $900^\circ\text{C}$ . They were then ground, pressed into pellets, and sintered several times in air at intermediate temperatures. The final sintering was done at  $1250^\circ\text{C}$  for 24 h, followed by very slow cooling ( $0.2^\circ\text{C}/\text{min}$ ) down to  $300^\circ\text{C}$  in order to improve the cationic ordering at the perovskite  $B$  site and the oxygen stoichiometry [10,11].

X-ray diffraction patterns were collected at room temperature (RT) using a Siemens D-5000 diffractometer and Cu  $K\alpha$  radiation, and were used to verify that our specimen was single phase with the expected peaks for a perovskite phase.

The neutron diffraction experiments were carried out at the high-flux reactor of the Institut Laue Langevin (Grenoble, France) using the D1B ( $\lambda = 2.52 \text{ \AA}$ ), D20 ( $\lambda = 2.41 \text{ \AA}$ ), and D2B ( $\lambda = 1.594 \text{ \AA}$ ) diffractometers. Using helium cryostats, neutron powder diffraction (NPD) patterns were collected at fixed selected temperatures and also following temperature ramps with heating ratios ranging between 0.25 and 2 K/min. Structural and magnetic Rietveld refinements were made using the FULLPROF program [12]. Crystallographic tools from the Bilbao Crystallographic Server [13–15] and the ISOTROPY software suite [16] were also used.

The magnetic response to dc and ac magnetic fields was measured using a superconducting quantum interferometer device (SQUID) and a Physical Properties Measuring System (PPMS) from Quantum Design. The ac magnetization was measured at the frequency value of  $\nu = 333$  Hz and 10 Oe of amplitude.

## III. RESULTS AND DISCUSSION

For determining the proportion of antisites (misplaced cations) high-resolution neutron diffraction was used, confirming a nearly perfect Mn/Ni ordered superstructure. In the Supplemental Material [17], Fig. S1 shows the refinement of

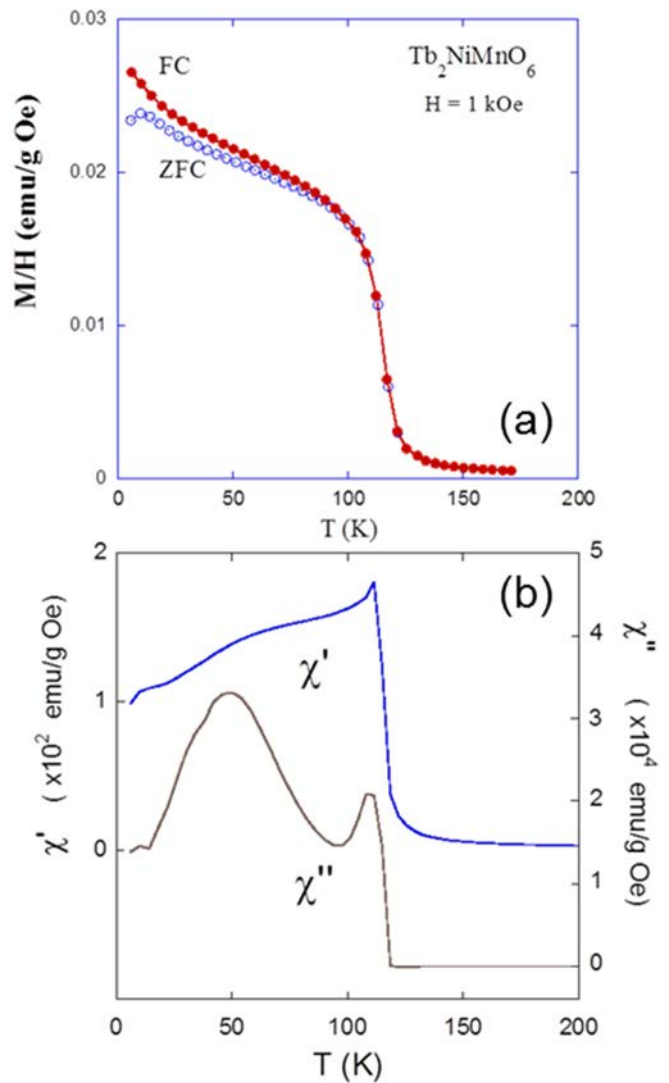


FIG. 1. (a) Comparison of the ZFC and FC dc magnetization measured under 1 kOe. (b) Temperature dependence of the in-phase ( $\chi'$ ) and out-of-phase ( $\chi''$ ) components of ac magnetic susceptibility for  $\text{Tb}_2\text{MnNiO}_6$  ( $h = 10$  Oe, 333 Hz) measured in FC.

the neutron pattern collected at 295 K (D2B). The structure refined in the paramagnetic and magnetically ordered phases agrees with a double perovskite with a monoclinic distortion ( $P2_1/n$  space group). The refinement of Mn/Ni occupancies in the  $B$  sublattice confirm a high ordering degree of around 98% so that antisite defects (ASDs) are  $\sim 2\%$  (50% means random Mn/Ni distribution). The refined interatomic Mn-O ( $\sim 2.053 \text{ \AA}$ ) and Ni-O ( $\sim 1.912 \text{ \AA}$ ) distances are close to the bond lengths expected for  $\text{Mn}^{4+}\text{-O}$  and  $\text{Ni}^{2+}\text{-O}$  [estimated bond valences  $+3.85(1)$  and  $+2.29(1)$ , respectively].

Magnetic and neutron measurements disclose the presence of several magnetic transitions at low temperature. The susceptibility of  $\text{Tb}_2\text{MnNiO}_6$  deviates from a Curie-Weiss evolution below  $\sim 200$  K (not shown), and the presence of ferromagnetism is easily identified below  $T_{C1} \sim 120$  K in the magnetization. Figure 1(a) displays the temperature dependence of dc magnetization under a magnetic field of 1 kOe in zero-field-cooled (ZFC) and field-cooled (FC) conditions.

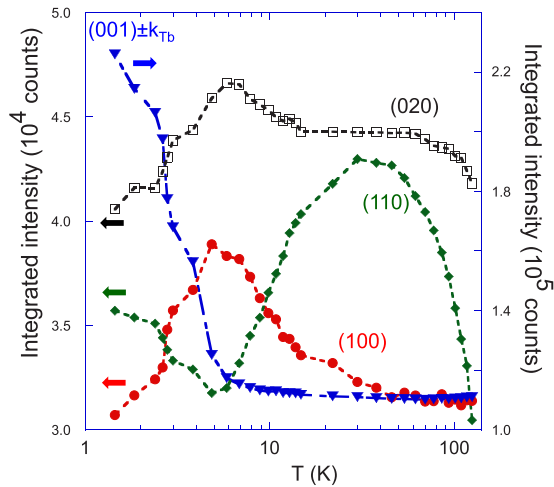


FIG. 2. Evolution down to 1.5 K of some selected integrated intensities corresponding to the main reflections with magnetic contribution: (100), (110), (020), and  $(001) \pm \mathbf{k}_{\text{Tb}}$ . Neutron measurements performed under heating on D1B. See explanation in the text.

These measurements reveal a tiny ZFC-FC magnetic irreversibility, in which the two branches meet and match one over the other below  $\sim 115$  K, coinciding with the ferromagnetic-like transition at  $T_{\text{C1}}$ . This ferromagnetic transition temperature is higher than in the homologous  $\text{Tb}_2\text{MnCoO}_6$  compound [18]. Compared to the dc magnetization, the sensibility to the magnetic behavior is higher in the ac magnetic response displayed in Fig. 1(b). Both the in-phase and out-of-phase signals are shown in this figure, which reveal a more complex scenario of magnetic phase transitions beyond the simple ferromagnetic ordering of Mn/Ni spins. In addition to the first maximum peaked at 110 K [Fig. 1(b)], the in-phase ac susceptibility ( $\chi'$ ) displays a second (very broad) maximum that in the out-of-phase component ( $\chi''$ ) extends over the 15–90 K range and it is peaked around 50 K. The presence on several kinks below  $T_{\text{C1}}$  foresees probable successive reorganizations of the spin ordering, as has been confirmed by neutron diffraction.

Figure 2 plots the evolution of the integrated intensity of four selected magnetic reflections between 1.5 and 120 K obtained after normalizing neutron data collected on D1B ( $\lambda = 2.52$  Å) warming the sample. In Fig. 3 we plot a  $T$ - $2\theta$  projection of the temperature dependence for the neutron-diffracted intensities around four characteristic magnetic reflections [(001)  $\pm \mathbf{k}_{\text{Tb}}$ , (100), (110), and (112)].  $\mathbf{k}_{\text{Tb}}$  in Figs. 2 and 3 reflects a very slight modulation (0.063[1], 0.069[1], 0.0387[2]) associated to defects in the arrangement of Tb moments (more details are given in the last paragraph of the current Sec. III). Figure 3 (top) shows the evolution in the high-temperature range (120–5 K), and in Fig. 3 (bottom) we show the corresponding evolution in the extended low-temperature range, between 1.5 and 12 K.

In order to describe the magnetic evolution one can distinguish two regimes: (i) the high-temperature one, in the 20–150 K temperature range, mainly governed by the magnetic metals at the  $B$  sites, and (ii) the changes occurring in the low-temperature range, below 15 K, where we expect the decisive intervention of the terbium moments.

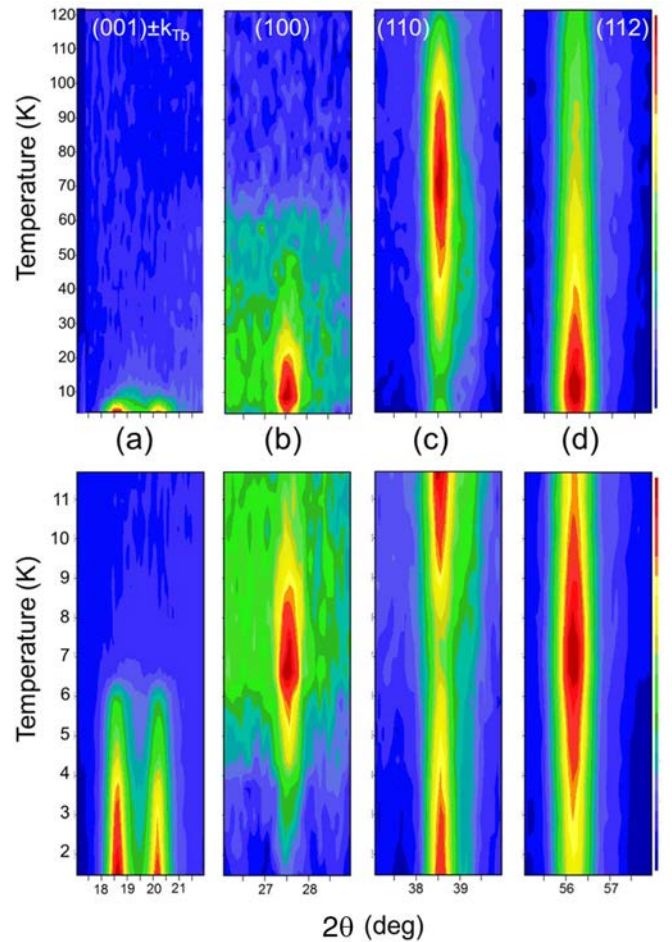


FIG. 3. Temperature evolution below 120 K of the NPD intensities (D1B) in four selected angular ranges around the magnetic reflections (a)  $(001) \pm \mathbf{k}_{\text{Tb}}$ , (b) (100), (c) (110), and (d) (112). Top: interval 120–5 K. Bottom: interval 12–1.5 K.

As we will show below, this almost perfectly ordered DP displays up to four different magnetic regimes. To explore possible symmetry breaks we used the tools freely available online at the Bilbao Crystallographic Server ([19]; also see [13–15]).

#### A. Evolution of the ferromagnetism in $B/B'$ sites down to 15 K

**FMI phase.** The structural description in the  $P2_1/n$  setting is displayed in the Supplemental Material [17] (see Table SI). The corresponding standard setting of this space group (SG) (No. 14) is  $P2_1/c$ , so that our nonstandard description of the parent space group is given in the nonconventional setting (**a**, **b**, **a** + **c**; 0, 0, 0). After examining possible magnetic space groups (MSGs) compatible with the gray group  $P2_1/c1'$  that keep unchanged the dimensions of the magnetic cell ( $\mathbf{k} = 0$ ), the magnetic intensities can be well reproduced by the maximal subgroup  $P2_1'/c'$  (No. 14.79 in BNS notation [20]). The magnetic ordering follows the irreducible representation (irrep)  $mGM_2^+$ , compatible with a magnetic arrangement of the  $F_x C_y F_z$  type in Bertaut's notation [21]. Figure 4 displays the refinement of the neutron pattern collected at 85 K, from which the ordered Mn moment

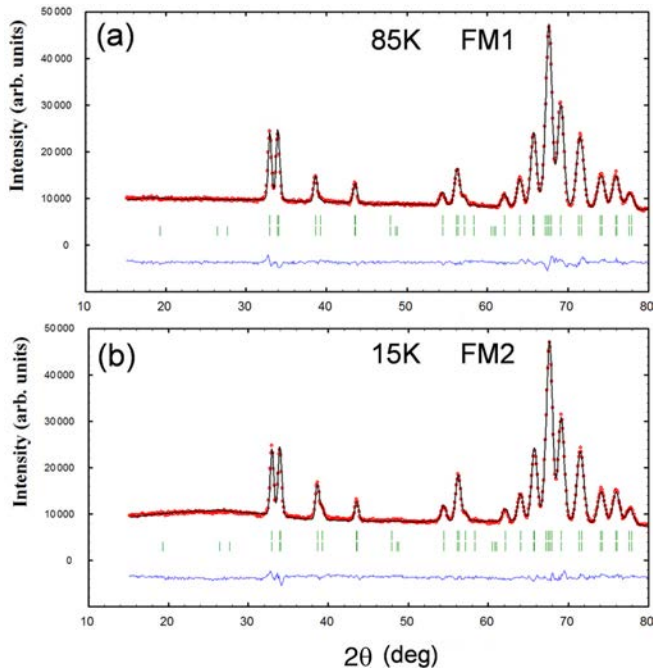


FIG. 4. Rietveld refinement (solid line) of the neutron patterns for  $\text{Tb}_2\text{MnNiO}_6$  collected on D1B at (a) 85 K (FM1 phase,  $\theta \approx 23[3]^\circ$ ), and (b) 15 K (FM2, rotating phase), using the  $P2'_1/c'$  MSG with  $\mathbf{m}[\text{Mn}] = 3/2 \mathbf{m}[\text{Ni}]$ .

is  $\mathbf{m}[\text{Mn}] = (0.85[8], 0, 1.85[4])\mu_B$  ( $m[\text{Mn}] = 2.03[5]\mu_B$ ), and  $\mathbf{m}[\text{Ni}] = (0.56[6], 0, 1.23[3])\mu_B$  ( $m[\text{Ni}] = 1.35[5]\mu_B$ ). In the refinements the  $\mathbf{m}[\text{Ni}]$  moment was constrained to  $2/3\mathbf{m}[\text{Mn}]$  according to the ratio  $S[\text{Mn}^{4+}]/S[\text{Ni}^{2+}] = 3/2$ . In the FM1 phase the  $F_z$  configuration is clearly dominant and the moments are almost parallel to the  $c$  axis of the perovskite. Spins make an angle  $\theta$  with the  $c$  axis of  $23[3]^\circ$  (and  $m_y = 0$ ).

**FM2 phase.** The FM1 order is stable within the  $[T_{C1}, T_{C2}] = [120 \text{ K}, 70 \text{ K}]$  temperature interval. Below  $\sim 70 \text{ K}$  neutron patterns evidence a gain of magnetic intensity in reflections of the type  $(0kl)$  and  $(hhl)$  with  $l \neq 0$  even, consistent with the strengthening of the  $F_x$  component as temperature is further reduced. In Fig. 3(c), top, the FM intensity in the (110) peak develops below  $T_{C1} \approx 120 \text{ K}$  but reaches a maximum around 70 K, coinciding with the appearance of a second maximum in the ac susceptibility, and then systematically decreases. This evolution illustrates first the emergence of the  $F_z$  component of the FM1 phase, but secondly, it shows that below  $\sim 70 \text{ K}$  there is a progressive and systematic transference of intensity from  $F_z$  to  $F_x$ . In this way, the aforementioned maximum in the (110) magnetic peak [red color in Fig. 3(c), top] signals the entering of the rotating FM2 phase. As the main feature of the FM2 regime, the FM moments progressively rotate towards the  $a$  axis upon cooling, causing a marked decrease of the (110) signal (and of  $m_z$ ) and the increase of the (112) magnetic intensity (and of  $m_x$ ) [Figs. 3(c) and 3(d), top]. Figure 5 plots the evolution of the (110) and (002) neutron magnetic intensities originated by, respectively, the  $F_z$  and  $F_x$  components, illustrating the strengthening of (002) when the former starts decreasing.

In this regime the single active  $mGM_2^+$  irrep is preserved and the neutron patterns were correctly reproduced by considering the  $P2'_1/c'$  MSG. Experimentally the  $y$  component is negligible at the  $B/B'$  sites. Mn and Ni exhibit a collinear order with their spins making an angle  $\theta$  with the  $c$  axis. The evolution of the tilting angle  $\theta$  down to 1.5 K is plotted in Fig. 6, where the evolution of the refined magnetic moments is depicted as well. In Fig. 4(b) we display the neutron pattern refined at 15 K and the extracted magnetic structure is shown in Table I. The tilting angle of the FM moments strongly depends on temperature below 60 K: At 15 K we found  $\theta = 46(2)^\circ$ . A schematic view of the evolution of the ferromagnetic structure and the anisotropic magnetization is shown as

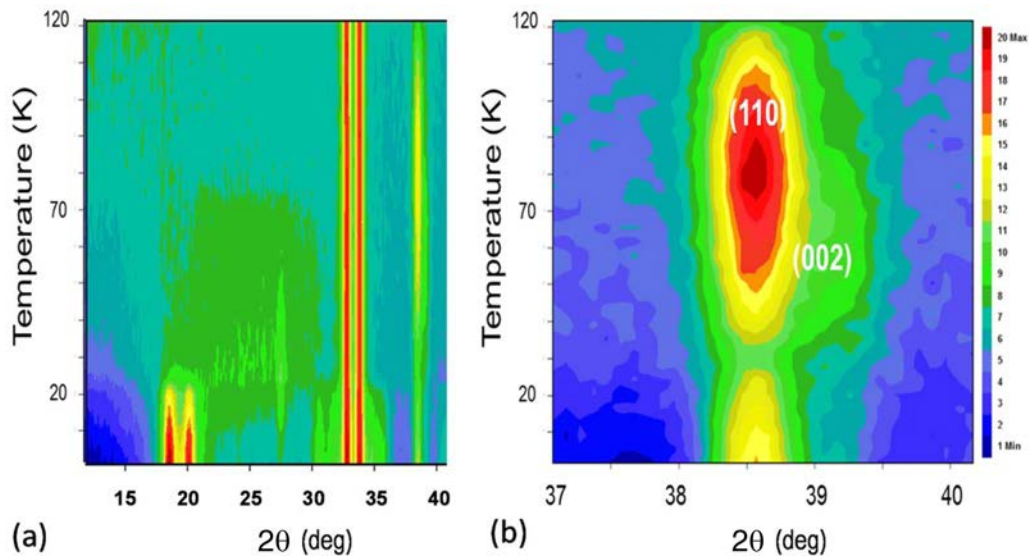


FIG. 5. Temperature evolution of neutron diffraction intensities (log scale) (a) at low angles showing the short-range ordering signal from Tb moments below 70 K, and (b) around (110) and (002) magnetic reflections. It shows the strengthening of the (002) peak below the maximum of (110), when the intensity of this one (associated to  $F_z$ ) decreases.

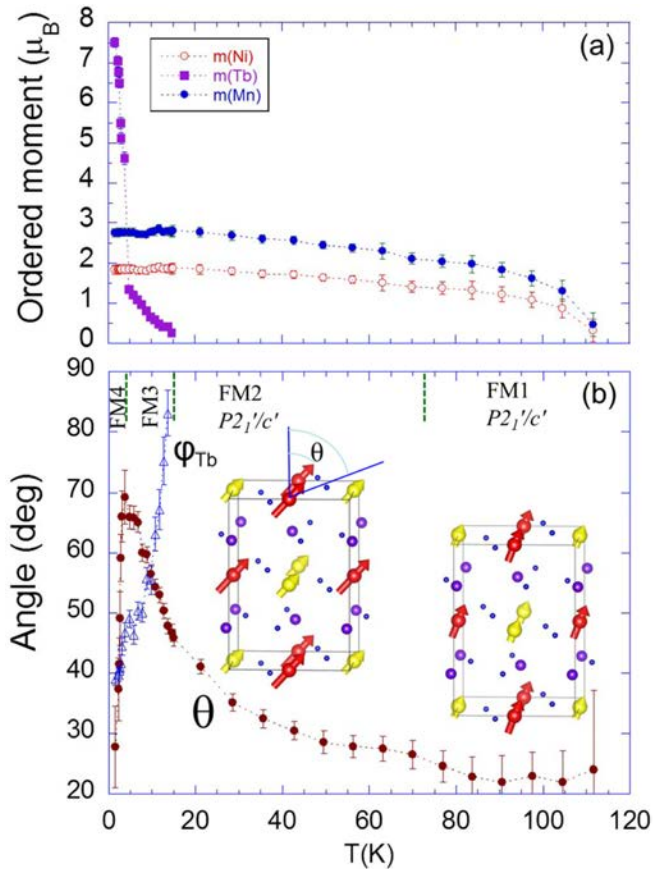


FIG. 6. (a) Temperature dependence of the ordered magnetic moments in  $\text{Tb}_2\text{MnNiO}_6$  refined from neutron patterns collected on D1B. At the  $B/B'$  sites moments were constrained according to the ratio  $S[\text{Mn}^{4+}]/S[\text{Ni}^{2+}] = 3/2$ . (b) Evolution upon increasing temperature of the angle  $\theta$  (circles) formed by the collinear  $3d$  metal moments (Mn/Ni) and the  $c$  axis. The evolution of the angle  $\varphi_{\text{Tb}}$  that Tb moments form with the  $a$  axis in the  $ab$  plane is also shown (blue unfilled triangles). In the inset we show the schematic view of the  $P2_1'/c'$  magnetic order in FM1 (above 80 K, with  $\theta$  small and constant) and FM2 phases. In the rotating FM2 phase the inclination angle ( $\theta$ ) systematically increases due to a significant ferromagnetic Tb-(Mn,Ni) interaction, which attracts metal moments towards the  $ab$  plane. The evolution of the canting in this phase is indicated in its corresponding figure.

insets in Fig. 6(b). Here we stress the fact that the Tb sublattice plays a key role on the evolution followed by the tilting angle ( $\theta$ ) of the magnetization. Figure 7 discloses the emergence of significant short-range ferromagnetic correlations between Tb moments, which are clearly visible below around 70 K, coinciding with the appearance of the rotating FM2 phase, the apparent augmentation of (002) magnetic intensity, and diminution of the (110) signal. So, these observations suggest and probably bear out that a ferromagnetic Tb-(Mn,Ni) interaction ( $J_{\text{Tb-M}} > 0$ ) is at the origin of the continuous rotation of the magnetization below  $T_{\text{C}2} \approx 70$  K. This interaction acts by attracting the metal moments towards the  $ab$  plane. Remarkably, as Fig. 6(b) discloses, the magnetization rotates  $\sim 50^\circ$  in the short interval 5–70 K.

Concerning the magnetism in the  $A$  site, Figs. 3 and 6 illustrate that slightly below 15 K the long-range ordering (LRO) of Tb moments is at play ( $T_{\text{N}3} \approx 15$  K).

### B. Successive magnetic phases with magnetic order at $A$ and $B$ sites below 15 K

In the two precedent ferromagnetic regimes (first with a very small stable canting, and later with the magnetization rotating with temperature) magnetic LRO is limited to  $B/B'$  sites. Two additional magnetic configurations were observed at lower temperatures that also involve the ordering of terbium moments at the  $A$  sites of this monoclinic perovskite. As we will see below, in both phases with ordered moments in  $A$  and  $B$  sites the resultant magnetization is non-null.

**FM3 phase.** The exchange field created by the  $3d$  metals at the  $A$  sites promotes the partial LRO of terbium moments below  $T_{\text{N}3} \approx 15$  K. Ostensible changes were observed in a set of reflections such as the (001)—forbidden by the structural  $P2_1/n$  symmetry—(100), (110), or (020) whose evolution is depicted in Figs. 2 and 3. So, for example, one can observe in Fig. 2 that the integrated intensity of (100) and (020) significantly grow on cooling between  $\sim 15$  K down to 6 K, by contrast with a marked decrease of the (110) signal. Note that the temperature evolution of the intensities does not follow a Brillouin curve, bearing out that the partial polarization of terbium moments is due to the FM exchange field created by the Mn/Ni sites. The refined neutron pattern at 6 K is shown in Fig. 7, and we show the details of the magnetic configuration in Table II. The evolution of magnetic order in the low-temperature range is depicted with great detail in Fig. 8. The tilting angle  $\theta$  of the metals, the refined moment in Tb atoms (perpendicular to  $c$ ), and its deviation with respect to the  $a$  axis (given by  $\varphi_{\text{Tb}}$ ) are shown down to 1.5 K. According to the symmetry dictated by the  $mGM_2^+$  irrep (or the  $P2_1'/c'$  MSG) the Tb moments adopt the permitted Bertaut  $F_x C_y F_z$  configuration [21]. The previous  $P2_1'/c'$  magnetic symmetry is preserved, in which all Tb sites are related by magnetic symmetry operations. Namely, Tb occupies a single independent position (Table II) and therefore the two Tb magnetic layers parallel to  $ab$  (at  $z \approx 0.25$  and  $z \approx 0.75$ ) are identical. The point magnetic symmetry is  $2'/m'$  (5.5.16), a *nonpolar* symmetry because this FM3 magnetic structure conserves the spatial inversion.

As can be deduced by inspection of the FM3 magnetic structure, the  $J_{\text{Tb-M}}$  exchange produces a mutual polarization: In addition to the partial polarization of Tb moments along the  $a$  axis, the tilting of the metal moments towards the  $ab$  plane becomes much more prominent below  $T_{\text{N}3}$ . So, we observe a significant increase of the canting angle  $\theta$  after entering the FM3 phase, which finally reaches a maximum of  $\theta_{\text{max}} = 70^\circ$  around 4 K, before decreasing again (Fig. 8).

**FM4 phase.** In  $\text{Tb}_2\text{NiMnO}_6$  the genuine magnetic ground state enters below  $T_{\text{N}4} \approx 3.7$  K, although its signature can be observed at higher temperatures in the form of short-range ordering (SRO) correlations. New magnetic reflections are visible, first as SRO and later as well-defined visible peaks around the positions (001), (011), (100), etc. (Figs. 2 and 3).

Accurate structural and magnetic refinements of neutron patterns collected below  $T_{\text{N}4}$  were obtained using the  $P2_1'$

TABLE I. Magnetic structures representative of the FM1 and FM2 regimes (refined at 75 and 15 K, respectively) in  $\text{Tb}_2\text{MnNiO}_6$  double perovskite. Parent space group in nonstandard setting ( $a, b, a + c; 0, 0, 0$ ).

$\text{Tb}_2\text{MnNiO}_6$	FM1, 75 K	FM2, 15 K
Magnetic space group	$P2'_1/c'$ (14.79)	$P2'_1/c'$ (14.79)
Transformation to standard setting	( <b>a, b, a + c; 0, 0, 0</b> )	( <b>a, b, a + c; 0, 0, 0</b> )
Magnetic unit cell	$a = 5.2728(2)$ $b = 5.5181(2)$ $c = 7.5104(3)$ $\beta = 90.165(4)^\circ$	$a = 5.2750(2)$ $b = 5.5167(2)$ $c = 7.5110(3)$ $\beta = 90.164(4)^\circ$
Magnetic point group	$2'/m'$ (5.5.16)	$2'/m'$ (5.5.16)
	Refined magnetic moments ( $\mu_B$ )	
Ni (0, 1/2, 0)	(0.56[6], 0, 1.23[3]) $m_T = 1.35(5)$	(1.25[4], 0, 1.22[4]) $m_T = 1.74(2)$
Mn (1/2, 0, 0)	(0.85[8], 0, 1.85[4]) $m_T = 2.03(5)$	(1.87[5], 0, 1.83[5]) $m_T = 2.61(2)$
	$\mathbf{m}[\text{Ni}] = 2/3 \mathbf{m}[\text{Mn}]$ ( $F_x, 0, F_z$ ) $\theta = 23(3)^\circ$	$\mathbf{m}[\text{Ni}] = 2/3 \mathbf{m}[\text{Mn}]$ ( $F_x, 0, F_z$ ) $\theta = 46(2)^\circ$

(4.9) MSG and the spin configuration described in Table II, which corresponds to the magnetic refinement of the neutron pattern collected at 1.5 K [Fig. 7(b)].  $P2'_1$  (4.9) is a direct subgroup (*translationgleiche*) of the  $P2'_1/c'$  (14.79) MSG, the common symmetry to the FM1, FM2, and FM3 ferromagnetic phases preceding the ground state of  $\text{Tb}_2\text{MnNiO}_6$ . Interestingly, the inversion symmetry operation connecting Tb magnetic ions at different  $\text{TbO}_2$  layers is lost. As a result of the  $P2'_1/c' \rightarrow P2'_1$  phase transition, the only Tb position in  $P2'_1/c'$  is split to give two independent Tb sublattices at low temperature (each of the Tb1 and Tb2 orbits corresponds to a different layer in the unit cell). Within the individual Tb layers the magnetic coupling is identical to the FM3 phase

generating a strong ferromagnetic component parallel to the  $a$  axis. What changes is that terbium moments in successive  $\text{TbO}_2$  layers (split sublattices) are now flipped, producing the cancellation of the ferromagnetic component ( $F_x C_y \rightarrow A_x G_y$ ). As a result, the ferromagnetic exchange field from Tb layers on the transition-metal layers (which was substantial in FM3) suddenly vanishes below  $T_{N4}$ . This cancellation of the  $4f$ - $3d$  exchange field felt by the  $B/B'$  metals permits a reentrant rotation back towards the  $c$  axis of the FM Mn/Ni spins, and so the angle  $\theta$  suddenly drops back to its position of comfort.  $\theta$  sharply decreases from  $\sim 70^\circ$  down to  $\sim 27^\circ$ , primarily dictated by the magnetic anisotropy of  $\text{Mn}^{4+}$  ( $t_{2g}^3 e^0$ ) and  $\text{Ni}^{2+}$  ( $t_{2g}^6 e^2$ ) metal ions. Remarkably, the canting of the magnetization in the ground state (1.5 K) adopts the same value ( $27^\circ$ ) as the initial value in the rotating FM2 phase [Fig. 6(b)]. Furthermore, Fig. 8 illustrates that across the FM3-to-FM4 phase transition the  $B$  cations experience strong changes in the competition between the anisotropic exchange (with origin at the FM Tb layers) and the single-ion anisotropy terms. As shown in this figure, this transition develops in two steps. First, the  $P2'_1/c' \rightarrow P2'_1$  symmetry breaking takes place by the inversion of half of the Tb layers ( $F_x C_y \rightarrow A_x G_y$  Tb modes), producing a sudden jump ( $\Delta m \approx 4\mu_B/\text{Tb}$ ) in the ordered Tb moment. Then a second step occurs which raises the Tb moments up to  $7.5\mu_B/\text{Tb}$ . Most interestingly, whereas the metal moments do not rotate across the first step, the second step is concurrent or is activated only when metal spins initiate the reentrant spin reorientation towards the  $c$  axis. Then, the magnetization in the Mn/Ni sublattices describes a sharp spin reorientation  $\Delta\theta \approx -43^\circ$  in only 1.5 K (on warming from 3 K down to 1.5 K).

The transition temperature  $T_{N4} \approx 3.7$  K coincides with the AF ordering temperature of terbium in other perovskites such as  $\text{TbCoO}_3$  ( $T_N = 3.3$  K [22]). Interestingly, the absence of moments at the  $B$  site in  $\text{TbCoO}_3$  (in the ground state  $\text{Co}^{3+}$  atoms are in  $LS, S = 0$ ) indicates that (apart from anisotropy terms)  $J_{\text{Tb-Tb}}$  must be very similar in the cobaltite and in  $\text{Tb}_2\text{MnNiO}_6$ . As in  $\text{TbCoO}_3$  the observed magnetic arrangement of Tb moments in the FM4 phase (ground state) reflects the Ising nature of the terbium moments associated

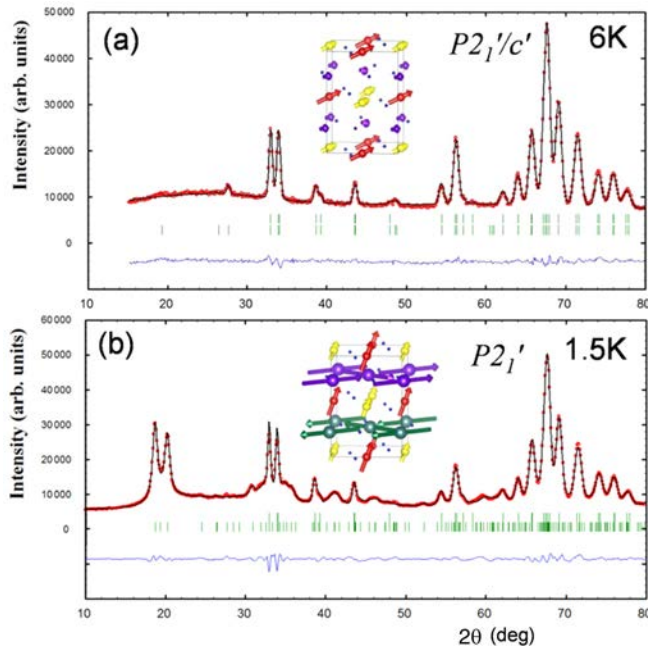


FIG. 7. Rietveld refinement (solid line) of the neutron patterns for  $\text{Tb}_2\text{MnNiO}_6$  collected on D1B at (a) 6 K (FM3 phase), and (b) 1.5 K (FM4 phase), using, respectively, the  $P2'_1/c'$  and  $P2'_1$  MSGs.

TABLE II. Magnetic structures representative of the FM3 and FM4 magnetic phases (refined at 6 and 1.5 K, respectively) in  $\text{Tb}_2\text{MnNiO}_6$  double perovskite.

$\text{Tb}_2\text{MnNiO}_6$	FM3, 6 K	FM4, 1.5 K
Magnetic space group	$P2_1'/c'$ (14.79)	$P2_1'$ (4.9)
Transformation to standard setting	( <b>a, b, a + c; 0, 0, 0</b> )	( <b>-c, b, a; 1/4, 0, 1/8</b> )
Magnetic unit cell	$a = 5.2750(3)$ $b = 5.5165(3)$ $c = 7.5113(3)$ $\beta = 90.164(4)^\circ$	$a = 5.2745(3)$ $b = 5.5164(3)$ $c = 7.5102(4)$ $\beta = 90.161(6)^\circ$
Magnetic point group	$2'/m'$ (5.5.16)	$2'$ (3.3.8)
Electric polarization tensor	–	Py
	Refined moments ( $\mu_B$ )	
Ni (0, 1/2, 0)	(1.64[5], 0, 0.76[5]) $m_T = 1.81(3)$	(0.8[2], 0, 1.6[1]) $m_T = 1.9[2]$
Mn (1/2, 0, 0)	(2.46[6], 0, 1.15[6]) $m_T = 2.72(4)$ $\mathbf{m}[\text{Ni}] = 2/3 \mathbf{m}[\text{Mn}] \quad \theta = 65(2)^\circ$	(1.3[3], 0, 2.4[1]) $m_T = 2.7[2]$ $\mathbf{m}[\text{Ni}] = 2/3 \mathbf{m}[\text{Mn}] \quad \theta = 27[6]^\circ$
Tb1 (0.017, 0.066, 0.749)	(0.76[4], 0.90[4], 0) $m_T = 1.18(4)$ ( $F_x, C_y, F_z = 0$ ) $\phi_{\text{Tb}} = 49.8[7]^\circ$	(5.84[6], 4.7[2], 0) $m_T = 7.5(1)$ $\phi_{\text{Tb1}} = \phi_{\text{Tb2}} = 39.9[5]^\circ$
Tb2 (0.982, 0.934, 0.250)		(-5.84[6], -4.7[2], 0) $m_T = -7.5(1)$

with the lowest crystal field energy levels. The electronic configuration of  $\text{Tb}^{3+}$  ions ( $4f^8$ ) determines its non-Kramers nature and strong anisotropy in low-symmetry sites. The

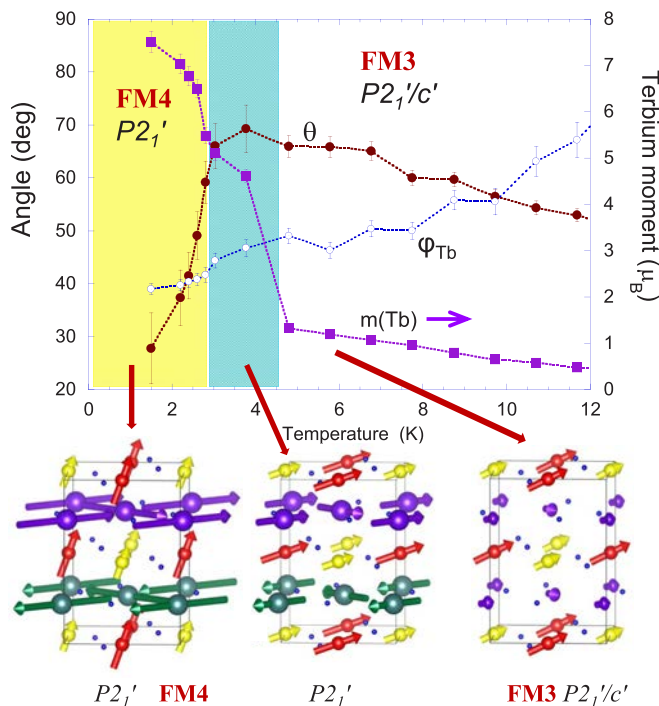


FIG. 8. Evolution of the magnetic order at A and B sites in the low-temperature range for  $\text{Tb}_2\text{MnNiO}_6$ . Evolution down to 1.5 K of the tilting angle  $\theta$  of the metals (filled circles, left axis), the refined moment in Tb atoms (filled squares, right axis), and the deviation  $\phi_{\text{Tb}}$  of Tb moments with respect to the  $a$  axis (unfilled circles, left axis). Lines are guides to the eye. Mn and Ni moments are fully ordered in this temperature range. A schematic view of the successive magnetic structures is also shown.

point-group symmetry of Tb in  $4e$  site is 1. As free ion its lowest-lying term is  ${}^7F_6$  ( $L = 3, S = 3, J = 6$ ). The low symmetry of Tb sites completely removes the degeneracy into 13 singlets [23,24], but the ground and first excited states of  $\text{Tb}^{3+}$  ions form an accidental quasidoublet, very close in energy ( $\Delta = 0.025$  meV for  $\text{TbAlO}_3$ ) [24], which involves two conjugate  $J = 6$  states of the type  $|6, +6\rangle + |6, -6\rangle$  and  $|6, +6\rangle - |6, -6\rangle$ . Any small external magnetic field or in this case the internal exchange field created by  $B/B'$ -site moments mix the two first eigenstates strongly favoring one of the  $|6, +6\rangle$  and  $|6, -6\rangle$  ionic states. As consequence the character of the  $\text{Tb}^{3+}$  moments is strongly Ising-like and they exhibit a very large local anisotropy.

In the polar  $P2_1'$  phase (FM4)  $J_{\text{Tb-Tb}}$  interactions promote an AF coupling between successive  $\text{TbO}_2$  layers and, as mentioned above, terbium moments exhibit strong Ising anisotropy within the  $x$ - $y$  plane. In this phase  $\text{Tb}^{3+}$  moments are ordered following the irrep ( $mGM_2^-$ ) whereas metal moments preserve the  $mGM_2^+$  magnetic mode. The Tb- $M$  ferromagnetic coupling expressed through the common  $F_x$  component in FM3 is overcome by Tb-Tb interaction producing the transformation of the  $F_x C_y$  Tb configuration (FM3) into  $A_x G_y$  (FM4), keeping the  $\text{Tb}^{3+}$  moments always in the  $x$ - $y$  plane due to the Ising anisotropy. In FM4  $\text{Tb}^{3+}$  moments in the same  $x$ - $y$  plane are noncollinear with their moments displaying almost  $90^\circ$  (Table II). On one hand, starting from the paramagnetic gray  $P2_1/n$  group, the activation of the magnetic  $mGM_2^+$  mode in Co/Ni sublattices generates a  $P2_1'/n'$  (14.79) nonpolar symmetry. On the other hand, the  $mGM_2^-$  mode adopted by  $\text{Tb}^{3+}$  moments below  $T_{N4}$  produces a  $P2_1'/n$  (14.77) symmetry, also *nonpolar*. However, even if these two distortion magnetic modes adopted, respectively, by the rare-earth and metal sites generate *nonpolar* symmetries ( $P2_1'/n'$  and  $P2_1'/n$  separately), the intersection of both groups produces the final  $P2_1'$  (4.9) MSG in which the loss of the  $n$  plane ( $c$  plane in the

$P2_1/c$  setting) causes the splitting of the Tb site (and each of the three oxygen positions) in two orbits and the disappearance of the inversion center  $\{-1|0\}$  at the origin of the parent phase. Therefore, the final ferrimagnetic FM4 configuration shown in Fig. 8 is *polar*, and its magnetic point symmetry  $2'$  (3.3.8) permits the appearance of ferroelectricity with spontaneous electrical dipoles parallel to the unique axis  $b$ .

An additional remarkable feature in the diffraction patterns below  $T_{N4}$  is the presence of defects in the stacking of ferrimagnetic Tb layers, so it is necessary to include a small modulation  $\mathbf{k}_{\text{Tb}} = (0.063[1], 0.069[1], 0.0387[2])$  associated to the ordering of  $\text{Tb}^{3+}$  moments. This modulation matches well the angular position of the magnetic intensities nearby (001) in the FM4 ground state. This smooth magnetic modulation superimposed to the primary  $A_xG_y$  mode of Tb moments has a very long period of  $\sim 200$  Å at 1.5 K perpendicular to the ferrimagnetic  $x$ - $y$  Tb layers. Within these layers the period of the modulation is around  $\sim 80$ – $90$  Å and it is rather isotropic. This accidental extra modulation of Tb moments is very soft or light, and it does not imply a significant alteration of the average and primary  $P2_1'$  magnetic symmetry of the FM4 phase in  $\text{Tb}_2\text{MnNiO}_6$ , whose tensor properties are dictated by the polar  $2'$  point symmetry.

#### IV. CONCLUDING REMARKS

$\text{Tb}_2\text{MnNiO}_6$  undergoes four magnetic transitions below room temperature. Two inverse spin reorientation transitions of the metal moments were observed with decreasing temperature, always keeping the ferromagnetic  $mGM_2^+$  configuration at the  $B$  sites: One is very slow and develops in the interval 70–4 K. The second, very sharp and opposite to the former, is concurrent to the activation of the  $A_xG_y$  mode of Tb moments during their  $mGM_2^+$  to  $mGM_2^-$  transition

( $T_{N4} \approx 3.7$  K). The ground state is ferrimagnetic and exhibits polar  $P2_1'$  symmetry so that ferroelectricity (induced by symmetric magnetostriction) and macroscopic magnetization can coexist in this perovskite. Spontaneous electric polarization is anticipated as a secondary effect induced by the superposition of primary nonpolar magnetic modes associated to the zone center in the reciprocal space. A large ferromagnetic component is preserved in the system ( $5 \mu_B/\text{f.u.}$ ), not related to a weak ferromagnetic (wFM) component induced by DM interaction. Although ferroelectricity and ferromagnetism would not be induced by the same instability, the overlay of the  $mGM_2^+$  ( $B$  site) and  $mGM_2^-$  ( $A$  site) modes generating the polar symmetry is accompanied by a sudden change in the anisotropy of the resulting ferromagnetism. A sharp reorientation of the magnetization concurs with the entering of the polar phase. Accordingly we can assure that the same instability (the substitution of  $mGM_2^+$  by  $mGM_2^-$  mode in the Tb sublattice) is finally responsible for the activation of the polar  $P2_1'$  symmetry and the severe rotation of the ferromagnetic vector. Consequently, the ferroelectric state could be switched off (on) by applying magnetic fields along  $a$  (along  $c$ ), and reversely, the orientation of the spontaneous magnetization could be severely modified by the application of voltages along the  $b$  axis (polar axis).

#### ACKNOWLEDGMENTS

We acknowledge ILL and D1B-CRG (Ministerio de Ciencia, Innovación y Universidades, MICIU, Spain) for beam time allocation. We thank financial support from the Spanish MICIU [Projects No. MAT2015-68760-C2-1, No. MAT2015-68760-C2-2, No. RTI2018-098537-B-C21, and No. RTI2018-098537-B-C22, cofunded by ERDF from EU, “Severo Ochoa” Programme (SEV-2015-0496)] and DGA (Grant No. E12\_17R).

- 
- [1] S. Goshen, D. Mukamel, and H. Shaked, *J. Appl. Phys.* **40**, 1590 (1969).
- [2] J. M. Perez-Mato, S. V. Gallego, L. Elcoro, E. Tasci, and M. I. Aroyo, *J. Phys.: Condens. Matter* **28**, 286001 (2016).
- [3] J. Blasco, J. L. García-Muñoz, J. García, G. Subías, J. Stankiewicz, J. A. Rodríguez-Velamazán, and C. Ritter, *Phys. Rev. B* **96**, 024409 (2017).
- [4] K. P. Belov, A. K. Zvezdin, A. M. Kadomtseva, and R. Z. Levitin, *Sov. Phys. Usp.* **19**, 574 (1976).
- [5] H. J. Zhao, L. Bellaiche, X. M. Chen, and J. Íñiguez, *Nat. Commun.* **8**, 1 (2017).
- [6] Y. Tokunaga, S. Iguchi, T. Arima, and Y. Tokura, *Phys. Rev. Lett.* **101**, 097205 (2008).
- [7] M. Kenzelmann, A. B. Harris, S. Jonas, C. Broholm, J. Schefer, S. B. Kim, C. L. Zhang, S.-W. Cheong, O. P. Vajk, and J. W. Lynn, *Phys. Rev. Lett.* **95**, 087206 (2005).
- [8] T. Kimura and Y. Tokura, *J. Phys.: Condens. Matter* **20**, 434204 (2008).
- [9] O. Prokhnenko, R. Feyerherm, M. Mostovoy, N. Aliouane, E. Dudzik, A. U. B. Wolter, A. Maljuk, and D. N. Argyriou, *Phys. Rev. Lett.* **99**, 177206 (2007).
- [10] T. Kymen, R. Yamazaki, and M. Itoh, *Chem. Mater.* **15**, 4798 (2003).
- [11] A. J. Barón-González, C. Frontera, J. L. García-Muñoz, B. Rivas-Murias, and J. Blasco, *J. Phys.: Condens. Matter* **23**, 496003 (2011).
- [12] J. Rodríguez-Carvajal, *Phys. B (Amsterdam, Neth.)* **192**, 55 (1993).
- [13] M. I. Aroyo, J. M. Perez-Mato, C. Capillas, E. Kroumova, S. Ivantchev, G. Madariaga, A. Kirov, and H. Wondratschek, *Z. Kristallogr.* **221**, 15 (2006).
- [14] J. M. Perez-Mato, S. V. Gallego, E. S. Tasci, L. Elcoro, G. de la Flor, and M. I. Aroyo, *Annu. Rev. Mater. Res.* **45**, 217 (2015).
- [15] M. I. Aroyo, A. Kirov, C. Capillas, J. M. Perez-Mato, and H. Wondratschek, *Acta Crystallogr., Sect. A: Found. Crystallogr.* **62**, 115 (2006).
- [16] B. J. Campbell, H. T. Stokes, D. E. Tanner, and D. M. Hatch, *J. Appl. Crystallogr.* **39**, 607 (2006).
- [17] See Supplemental Material at <http://link.aps.org/supplemental/10.1103/PhysRevB.99.184444> for crystal structure determination from neutron diffraction at room and low temperatures.
- [18] J. Blasco, J. García, G. Subías, J. Stankiewicz, S. Lafuerza, J. A. Rodríguez-Velamazán, C. Ritter, and J. L. García-Muñoz, *J. Phys.: Condens. Matter* **26**, 386001 (2014).
- [19] <http://www.cryst.ehu.es>

- [20] N. V. Belov, N. N. Neronova, and T. S. Smirnova, *Sov. Phys. Crystallogr.* **2**, 311 (1957).
- [21] E. F. Bertaut, *Acta Crystallogr., Sect. A* **24**, 217 (1968); Bertaut modes ( $F$ ,  $A$ ,  $C$ ,  $G$ ) are defined by ordering the Tb atoms according to the symmetry operations (1)  $x, y, z$ ; (2)  $-x, -y, -z$ ; (3)  $-x, y + 1/2, -z + 1/2$ ; (4)  $x, -y + 1/2, z + 1/2$ .
- [22] K. Knížek, Z. Jiráček, P. Novák, and C. De La Cruz, *Solid State Sci.* **28**, 26 (2014).
- [23] J. B. Gruber, K. L. Nash, R. M. Yow, D. K. Sardar, U. V. Valiev, A. A. Uzkov, and G. W. Burdick, *J. Lumin.* **128**, 1271 (2008).
- [24] P. Novák, K. Knížek, and J. Kuneš, *Phys. Rev. B* **87**, 205139 (2013).